# LANGMUIR

pubs.acs.org/Langmuir Article

# Surface-Mediated Self-Assembly of Kinetoplast DNA: Depletion-Driven Dimer Formation and Quasi-2D Dynamics

Zahra Zarei, Indresh Yadav, and Patrick S. Doyle\*



Cite This: https://doi.org/10.1021/acs.langmuir.5c04422

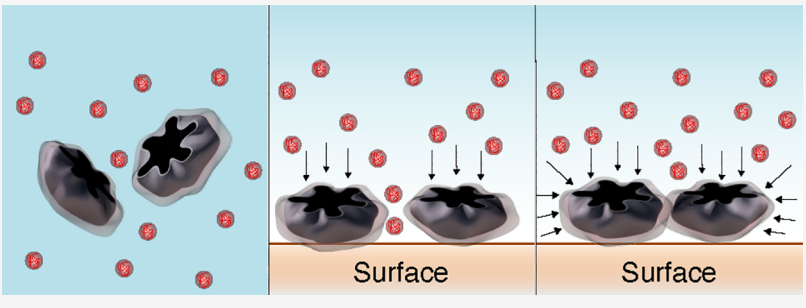


**ACCESS** I

III Metrics & More

Article Recommendations

s Supporting Information



ABSTRACT: Depletion interactions play a crucial role in the assembly and dynamics of colloidal systems in polymer-rich environments. In this study, we investigate the behavior of asymmetric, soft, colloidal kinetoplast DNA (kDNA) in the presence of linear polymers (linear DNA), focusing on their surface accumulation, orientation, diffusion, and dimer formation. We observe that the kDNAs preferentially migrate to a solid surface with a preferred orientation due to depletion interactions with the substrate, a phenomenon absent in polymer-free conditions. Over time, the kDNAs adopt a stable orientation at the surface, and the orientation of individual kDNAs on the surface adopts a polar order. By analyzing kDNA diffusion both in bulk and on the surface, we find that surface-bound kDNAs exhibit prolonged confinement within the field of view, while bulk kDNAs rapidly diffuse out of view. Additionally, we observe the formation of dimers as kDNAs encounter each other on the surface, driven by depletion forces. The kDNAs within the dimers are able to rotate relative to each other and deform to maximize their interaction energy. Fluorescent labeling of both the polymers and kDNAs reveals polymer exclusion from the kDNA-surface and inter-kDNA regions, confirming depletion-driven attraction. We quantified the depletion attraction by measuring the excluded volume between dimerized kDNAs using confocal fluorescence microscopy. These findings provide insights into depletion-mediated interactions in soft, asymmetric colloids and further establish kDNA as a model system for studying the colloidal behavior of catenated soft particles.

# INTRODUCTION

In soft matter and biological systems, short-range interactions, whether directional or entropic, control the spatial organization of dispersed components at equilibrium. Among these, short-range depletion interactions play significant role for organization in biological systems and engineered colloids, driving assembly through entropic forces that can be controlled or replicated. These depletion interactions, entropic in origin, arise from the exclusion of nonadsorbing particles or polymers between colloids or surfaces, generating an effective attraction whose range and strength can be controlled independently. Their tunability makes them a powerful tool for directing assembly across scales, from biological tissues to synthetic materials.

Various naturally occurring and custom-shaped colloids have been observed to self-assemble into complex structures due to depletion forces. One example in nature is the aggregation of biconcave red blood cells that tend to aggregate with their flat sides facing each other, like a stack of coins (rouleaux).<sup>2</sup> Another striking example is the morphogenesis of bacterial

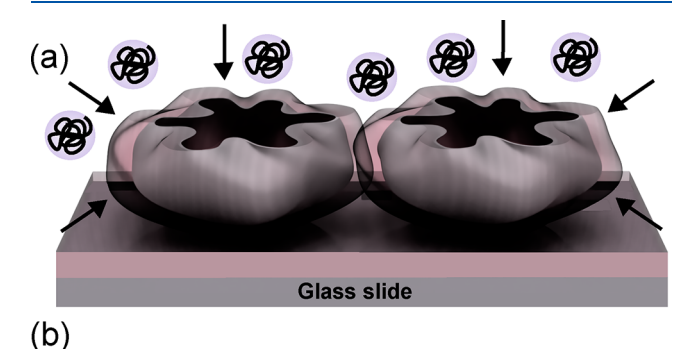
cables in polymeric environments.<sup>3</sup> In crowded cellular environments, depletion forces mediate essential processes from genome organization to liquid—liquid phase separation. When dysregulated, these entropic interactions can drive pathological protein aggregation underlying neurodegenerative diseases such as Alzheimer's, Parkinson's, and ALS.<sup>4–8</sup> For colloidal science, depletion interactions offer even greater potential, as their strength and directionality can be programmed through particle design. By tuning shape, size, and flexibility, researchers can encode specific assembly pathways without complex chemical modifications. This programmability has made colloidal self-assembly a cornerstone of materials science.<sup>9</sup> While selective binding (e.g., DNA

Received: August 25, 2025 Revised: November 4, 2025 Accepted: November 4, 2025



hybridization) enables precise crystallization, $^{10-14}$  and surface patterning introduces directional interactions, $^{15-17}$  such approaches often require complex synthesis. In contrast, shape anisotropy provides a simpler route to control assembly. Nonconvex particles, ellipsoids, bowls, or dimpled colloids, leverage depletion forces to form hierarchical structures through entropic effects alone. 18-22 Notably, shape-complementary particles exhibit emergent lock-and-key behavior even without predefined binding sites. Surface roughness or indentations modulate excluded-volume overlaps, enabling particles to interlock under depletion attraction. <sup>23–26</sup> Confinement further enhances this directional control, as seen with anisotropic particles at interfaces.<sup>24</sup> Depletion forces can also deform soft boundaries, for example changing the shape of vesicles containing hard Brownian spheres.<sup>27</sup> These systems demonstrate how physical design, rather than chemical specificity, can guide self-assembly and open scalable routes to functional materials.

Previous studies have primarily focused on rigid or preshaped colloids. Herein we focus on soft, flexible colloids whose shape adapts dynamically during assembly. We make use of a flexible colloid synthesized in nature, kinetoplast DNA (kDNA) from *Crithidia fasciculata*. kDNA is a 2D polymer network that spontaneously adopts positive Gaussian curvature in solution <sup>28–30</sup> (Figure 1). Unlike lipid bilayers, isolated



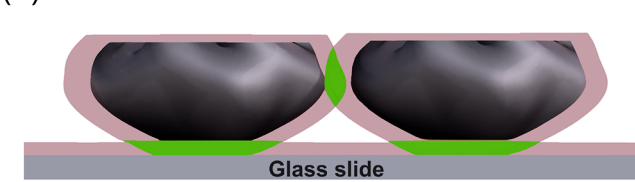


Figure 1. Schematic of a kDNA dimer on a surface, showing depletion layers and excluded volume overlap. (a) Top view of a base-down kDNA dimer, with depletion layers (pink) between kDNAs, and between kDNA and solid surface (glass slide). (b) Side view of the dimer, illustrating the excluded volume overlap (green) and depletion regions (pink).

kDNA in solution forms stable, wrinkled hemispherical morphologies ("shower caps") while retaining its 2D polymeric structure. This unique material is a catenated network of  $\sim\!5000$  DNA minicircles (2.5 kbp) and  $\sim\!25$  DNA maxicircles (40 kbp) topologically interlocked in a quasi-2D plane, with minicircles exhibiting a catenation valency of  $\sim\!3$ .

kDNA offers unique advantages over conventional soft colloids (e.g., vesicles or erythrocytes). Its polymeric nature enables precise tunability: enzymatic digestion modulates stiffness, <sup>35</sup> size tuned by ionic strength, <sup>36</sup> and conformation adjusted through the introduction of polymers smaller than the kDNA mesh size <sup>37</sup> which is 34 nm. <sup>38,39</sup> Our choice of  $\lambda$ -DNA

as the depletant is multifold. First, recent work by our group has suggested that  $\lambda$ -DNA can drive kDNA to assemble into aggregates through depletion interactions, though quantification of these interactions is lacking. Furthermore,  $\lambda$ -DNA and kDNA can be separately stained with spectrally distinguishable dyes and their relative positions imaged in a mixture using fluorescence microscopy. Use of an all DNA system also focuses the study on the role of topology and polymer size, rather than specific chemical interactions among the species. Unlike conventional lock-and-key systems with fixed geometries, kDNA combines anisotropy, flexibility, and curvature, enabling continuously tunable depletion-driven interactions. This interplay between softness, edge roughness, curvature, and depletion forces creates novel assembly pathways inaccessible to rigid particles.

Beginning with single-particle microrheology of individual kDNA, we characterize collective assembly and quantify depletion-mediated dimer interactions. Key findings reveal that depletion interactions drive kDNA to surfaces dominated by a base-down orientation, where they exhibit quasi-2D diffusion with reduced mobility compared to bulk. Surface confinement stabilizes dimerized states, preventing detachment and enabling high-resolution tracking. Our quantification of these interactions uncovered metastable dimers, which dynamically form and dissociate in the presence of weak depletion forces. Observations reveal that dimers maintain aligned orientation with respect to the surface while their components dynamically glide and rotate relative to each other. These results demonstrate that depletion interactions can be leveraged to control the assembly of soft, shapeadaptive colloids at interfaces. Our system provides a unique platform to directly observe colloidal conformations and dynamics over long time scales, yielding fundamental insights into reconfigurable soft matter assembly.

# MATERIALS AND METHODS

Sample Preparation. Kinetoplasts (kDNA) from trypanosomatid Crithidia fasciculata were purchased from TopoGEN Inc. Received kDNA solution has a concentration of 1120  $\mu$ g mL<sup>-1</sup>. The solvent was TE buffer, which is composed of 10 mM Tris-HCl, pH 7.5, and 1 mM EDTA. Bacteriophage λ-DNA (48.5 kbp, contour length of 16.5  $\mu$ m) was purchased from New England Biolabs, Ipswich, MA. As received from the manufacturer the  $\lambda$ -DNA stock solution has a concentration of 500  $\mu g$  mL<sup>-1</sup>. The solvent was TE buffer, which is composed of 10 mM Tris-HCl, pH 8.0, and 1 mM EDTA. To remove naturally formed concatemers of  $\lambda$ -DNA, the stock solution was heated to 65 °C for 10 min, then rapidly cooled to 23 °C by immersion in a water bath. To have a stronger binding of the dye molecules to kDNA and overcome the influence of ionic strength on the dye-DNA interaction kinetics, we used MFP488 MIRUS dye which binds covalently to nucleotides. $^{40,41}$  The staining ratio of the dye molecule to the kDNA base pair was about 1:160. We visualize the  $\lambda$ -DNA using Cy5. By choosing Cy5 we ensured sufficient separation between the emission and excitation spectra of these two dyes to obtain high-quality data from each imaging channel independently. The reaction protocol was adopted as suggested by the manufacturer for both  $\lambda$ -DNA and kDNA, however, a purification protocol was developed. After the binding reaction was completed, both samples were centrifuged in 100 kDa cutoff membrane (Amicon Ultra Centrifugal Filter, Merck) at room temperature at 5000g for 5 times and each run for 2 min to remove the unbound dye and redisperse the sample in 0.5× TBE buffer. Glass coverslips were cleaned with ethanol and soaked at least 1 h in 1 M NaOH. Samples were imaged inside a microwell created on microscope coverslip using Frame Seal Slide Chambers purchased from Bio-Rad Laboratories.

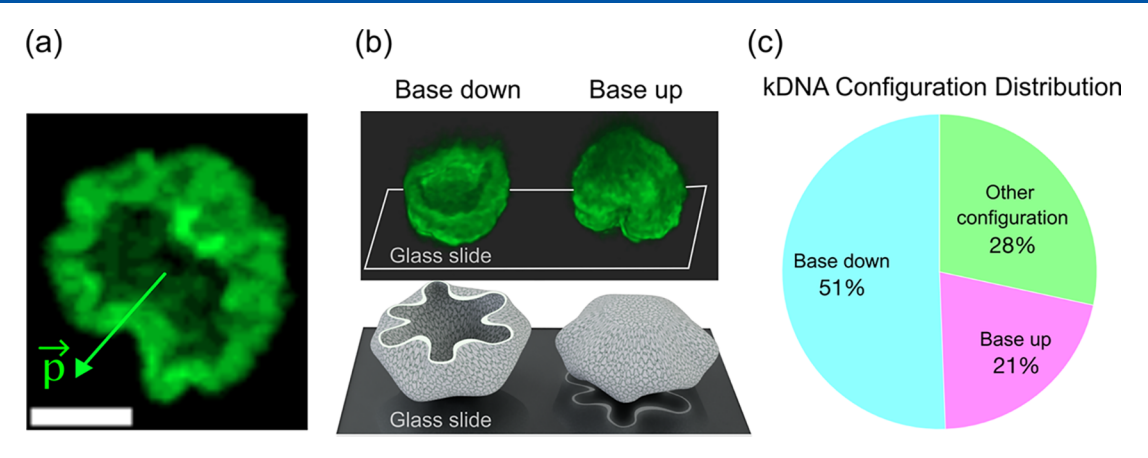


Figure 2. 3D structure and orientation preferences of kDNA on a solid surface. (a) 3D reconstruction of kDNA in bulk from confocal z-stack images. The green unit vector  $\overrightarrow{p}$  represents the orientation of kDNA (base-to-top axis). (b) (top) 3D reconstruction from confocal microscopy images of kDNA on a glass slide (surface) using Imaris, shown from a slightly tilted side view. (bottom) Schematic representation of each kDNA orientation (base down, base up) on the glass slide. (c) Pie chart showing the percentage distribution of each kDNA orientation (base down, base up, and other configurations) on the surface. Scale bar is 2  $\mu$ m.

Assembling Experiment. We first prepare sample of kDNA containing 100  $\mu$ g mL<sup>-1</sup>  $\lambda$ -DNA. In this system, attractive forces between kDNAs arise due to depletion interactions mediated by  $\lambda$ -DNA acting as a polymer in the solution. Simultaneously, electrostatic repulsion between charged DNA molecules also plays a significant role. By screening the electrostatic repulsion, the attractive depletion interactions become dominant, thereby influencing the overall phase behavior of the system. The system is investigated at physiological pH in tris-boric acid-ethylenediaminetetraacetic acid (0.5 $\times$  TBE) buffer with an ionic strength of 32.3 mM. $^{36}$  To screen the Coulombic repulsions between the DNA chains, an additional 25 mM of NaCl is added. Thus, the resultant ionic strength of the solution is 57.3 mM corresponding to a Debye length of 1.27 nM compared to the 2 nM bare width of dsDNA. We prepare a dilute sample of kDNA containing 100  $\mu$ g mL<sup>-1</sup>  $\lambda$ -DNA and 1  $\mu$ g mL<sup>-1</sup> kDNA. The solution containing the stained kinetoplast (kDNA) molecules was mixed with partially stained  $\lambda$ -DNA, where 30–40% of the  $\lambda$ -DNA was stained, and the remaining  $\lambda$ DNA was unstained. Samples were gently mixed using wide-cut tips. For each sample, a 25  $\mu L$  volume was placed inside a well measuring 9 mm × 9 mm in length and width, with a depth of 310  $\mu$ m.

Fluorescence Imaging. We employed a super-resolution laser scanning confocal microscope. A Zeiss LSM 980 with Airyscan 2 microscope was used in oil-immersion mode with a 63× objective (numerical aperture 1.4). For 3D visualization of kDNA, Fluorescence images were acquired at sequential z-planes with a z-step of 160 nm, then assembled into a volumetric rendering using Fiji (ImageJ) or Imaris (Oxford Instruments, Version 10.2) to visualize the kDNA structure. Images were acquired at the bottom of the chamber, just above the coverslip. The captured images were analyzed using ImageJ and custom-built scripts in MATLAB (MathWorks, Natick, MA).

## EXPERIMENTAL RESULTS

To understand how depletion forces affect kDNA, we divide our study into two parts. First, in the Single kDNA Behavior section, we resolve how individual kDNAs respond to their environment by probing surface alignment, bulk diffusion, and interfacial mobility, ultimately revealing  $\lambda$ -DNA's influence on isolated kDNAs. Second, in the Pairwise Assembly section, we explore dimer formation and dynamics, quantifying kDNA–kDNA interactions mediated by  $\lambda$ -DNA.

**Single kDNA Behavior.** *kDNA Accumulation on a Solid Surface with a Polar Order.* The adsorption of colloidal particles on soft surfaces plays a key role in biological processes, with well-established physics for both soft<sup>42–45</sup> and solid interfaces. <sup>46</sup> While concave, anisotropic particles and patchy colloids have been extensively studied<sup>47,48</sup> the behavior of soft, anisotropic, shape-adaptive kDNA on solid substrates remains unexplored. Here, we investigate how  $\lambda$ -

DNA-induced depletion forces mediate the assembly of kDNA on a glass slide.

As predicted by Asakura-Oosawa (AO) theory,  $^1$   $\lambda$ -DNA acts as a depleting agent, creating depletion layers around each kDNA and adjacent to the substrate interface. Diffusion brings kDNA close to the surface, where these layers begin to overlap, inducing short-range attractive forces. As the overlap increases, the depletion interaction strengthens; once exceeding  $k_{\rm B}T$ , kDNA bind irreversibly, transitioning from bulk diffusion to an adsorbed state (details on depletion mechanisms are provided in Pairwise Assembly section, Quantitative Analysis subsection). The presence of  $\lambda$ -DNA in the solution promotes thermodynamically favored orientations of adsorbed kDNA, as observed experimentally.

To investigate whether gravity or depletion interactions caused kDNA to gather at the surface, we conducted a control experiment by suspending kDNA in a buffer without  $\lambda$ -DNA and monitored its distribution over 4 h. According to Stokes' law, gravity-driven sedimentation should occur faster in water due to its lower viscosity. However, z-stacks confirmed a homogeneous dispersion with no sedimentation observed (Figure S1). To quantitatively characterize the effect of gravity relative to thermal energy, we calculated the gravitational height in both the presence and absence of  $\lambda$ -DNA to be  $\sim$ 63  $\mu$ m (see Supporting Information). This value is significantly larger than the size of a kDNA molecule ( $\sim$ 5  $\mu$ m) and constitutes a substantial fraction of the channel height (310  $\mu$ m). The addition of  $\lambda$ -DNA at this concentration causes a negligible change in solution density and thus an imperceptible change to the gravitational height. This confirms that gravitational effects were not important in our experimental conditions and that adsorption in our system arises solely from depletion interactions. Next, we characterize the microscopic orientation of individual kDNA molecules at the interface.

The kDNA's orientation is fully described by a single unit vector  $\overrightarrow{p}$ , defined along the base-to-top axis of the cup-shaped structure, as shown in green in Figure 2a. While the majority of kDNAs retain their initial adsorption orientation, a subset undergoes reorientation at the beginning of the experiment. Tracking 20 kDNAs with varying orientations for 30 min confirmed no further reorientation once equilibrium was reached at around 4 h (Figure S2). Interestingly, the kDNA adopt a polar order: 51% of kDNAs adopt a base-down orientation ( $\overrightarrow{p}$  pointing away from the surface; Figure 2), while the remaining population adopts base-up ( $\overrightarrow{p}$  pointing into the surface) or other configurations ( $\overrightarrow{p}$  neither pointing out nor into the surface), typically oriented on their side or partially folded.

The equilibrium orientation is determined by excluded volume maximization: the thermodynamically favored base-down configu-

ration optimizes total excluded volume between kDNA and the substrate. Conversely, the base-up orientation brings the rim of the cup-shaped kDNA in contact with the surface which geometrically leads to less excluded volume. This energetic hierarchy is further modulated by kDNA's intrinsic flexibility. In the base-down orientation, interfacial contact flattens the cup-shaped kDNA at the adhesion site while the rim maintains curvature. In the base-up orientation, the kDNA's convex base faces away from the surface, resulting in only edge contact that preserves its full domed curvature (cross sections of both orientations are shown in Figures S3 and S4). Thus, the system exhibits orientational alignment of kDNAs, forming emergent polar order normal to the surface despite lacking positional order. Similar principles govern other anisotropic colloids: for example, tuning the density of surface ligands alters the balance between nanorod-interface and nanorod-nanorod depletion attractions, resulting in upright bundles, multilayered belts, or monolayer smectic phases,<sup>49</sup> and filamentous viruses exhibit liquid crystallinity through entropic effects.<sup>50</sup>

Having established how depletion forces govern kDNA's surface orientation, we now examine how these interactions influence its mobility, first in bulk solution and subsequently near interfaces, where confinement alters diffusive behavior.

Bulk Diffusion and Interfacial Mobility of kDNA. Once kDNAs adsorb to the surface in their preferred base-down orientation, their two-dimensional diffusion reflects the continued influence of depletion interactions at the interface. To better understand these effects, we first characterize kDNA's mobility in bulk solution (in the presence of  $\lambda$ -DNA) and then compare it with its behavior at the surface. In the bulk polymeric solution, kDNA's three-dimensional mobility was analyzed by tracking its translational diffusion and calculating the mean square displacement in 2D (projected from 3D motion). Movies show that kDNA exhibits rotational and translational diffusion, with its orientational vector  $\overrightarrow{p}$  continuously reorienting over time. Although slow, the diffusion of kDNA driven solely by thermal energy causes it to move out of the focal plane during the course of measurement (Figure 3a). In contrast, surface-adsorbed kDNA show fundamentally different behavior. Confined to twodimensional diffusion, the kDNAs maintain their orientation while diffusing laterally, parallel to the surface (Movie S1). Although minor fluctuations in the normal vector orientation occur, the overall orientation remains stable during the entire 25 min of data acquisition (Figure 3b).

The key difference between bulk and surface dynamics lies in their degrees of freedom. In bulk, kDNA explores six degrees of freedom (three translational, three rotational), resulting in unconstrained 3D diffusion with continuous reorientation and transient focal-plane trajectories due to rapid out-of-plane motion. On the surface, however, depletion forces restrict motion to just three degrees of freedom (two translational in-plane, one azimuthal rotation), leading to persistent 2D diffusion with complete focal-plane confinement. This distinction is evident in the long, continuous trajectories observed at the interface. The corresponding XY trajectories for both bulk and surface conditions are plotted in Figure 3b, with an additional surface trajectory provided in the Supporting Information, Figure S5).

To further characterize these dynamics, we quantified mobility of kDNA by analyzing the mean square displacement (MSD),  $r^2$ , in both bulk (projected XY motion) and on the surface (Figure 4). Interpreting diffusion requires estimating the viscosity of the  $\lambda$ -DNA solution. However, due to kDNA's nonspherical shape, viscosity cannot be directly derived from its radius and diffusion coefficient. We determined  $\lambda$ -DNA solution viscosity from bulk diffusion of 1  $\mu$ m tracer beads. Measured bead displacements are Gaussian and MSD scales linearly with lag time which confirms standard Brownian motion and a mostly viscous fluid (over this lag time scale). Long-time diffusivity D was obtained from the MSD slope via  $\langle r^2(\tau) \rangle = 4D\tau$ , where  $r(\tau)$  is displacement at the lag time  $\tau$ . The brackets represent time and ensemble averaging. Using the Stokes–Einstein relation, we calculated the  $\lambda$ -DNA solution viscosity as 2.46 mPa·s.

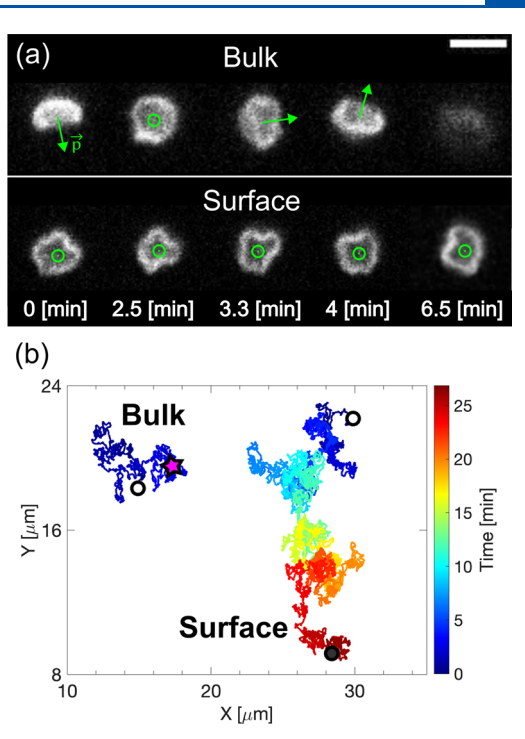


Figure 3. Diffusion of kDNA in bulk and on a solid surface. (a) Top: Snapshots showing the rotation and different orientations of kDNA in bulk while diffusing over time. Bottom: kDNA on the surface diffusing and rotating in-plane over time while maintaining its orientation on the surface. The orientation is fully described by a single unit vector  $\overrightarrow{p}$ , from the base of kDNA to the top. The vector pointing out of the plane (denoted by ⊙) represents the direction normal to the surface, oriented toward the viewer (Movie S1). (b) Trajectories of two typical kDNAs, one in the bulk and the other on a solid surface. The empty circle represents the beginning, the filled purple star shows the end of the trajectory for the kDNA in bulk while the filled circle represents the end of the trajectory for the kDNA on the surface. The colormap indicates time, with the trajectory color-coded to show movement over time. The kDNA in bulk leaves the field of view after 6 min, whereas kDNA on the surface stays attached without leaving the surface during the entire 25 min recording period. Recording was stopped at 25 min. The scale bar is 5  $\mu$ m.

Our measured viscosity is consistent with previous reports for entangled  $\lambda$ -DNA solutions at lower ionic strength<sup>51</sup> (see Supporting Information for the comparison).

We next measured kDNA diffusion in bulk solution (away from the surface). Similar to bead measurements in bulk, the MSD of kDNA increased linearly over the measured lag time. Using the solution viscosity obtained from spherical bead microrheology (2.46 mPa s), we calculated a kDNA hydrodynamic radius,  $R_{\rm H}$ , of 2.69  $\mu m$ . This  $R_{\rm H}$ closely matches the largest physical dimension of the cup-shaped kDNA previously reported<sup>28</sup> (half major axis length of 2.77  $\mu$ m, see SI). The close match between  $R_{\rm H}$  and kDNA's physical dimensions suggests that kDNA interacts with the solution in the same manner as a solid impenetrable bead and does not experiencing appreciable threading of linear DNA through its pores (see Supporting Information, Figure S6). In a threaded scenario, where  $\lambda$ -DNA strands penetrate and transiently constrain kDNA's motion, the kDNA would entangle with the background  $\lambda$ -DNA network, leading to significantly slower diffusion. Such threading would increase hydrodynamic drag, yielding a R<sub>H</sub> larger than kDNA's physical dimensions. We would also expect that threaded linear DNA would give rise to a nonlinear MSD for kDNA as it introduces a new unthreading time scale.

We next studied the surface-confined diffusion of spherical beads and compared it to that of kDNA in the presence of  $\lambda$ -DNA. Both

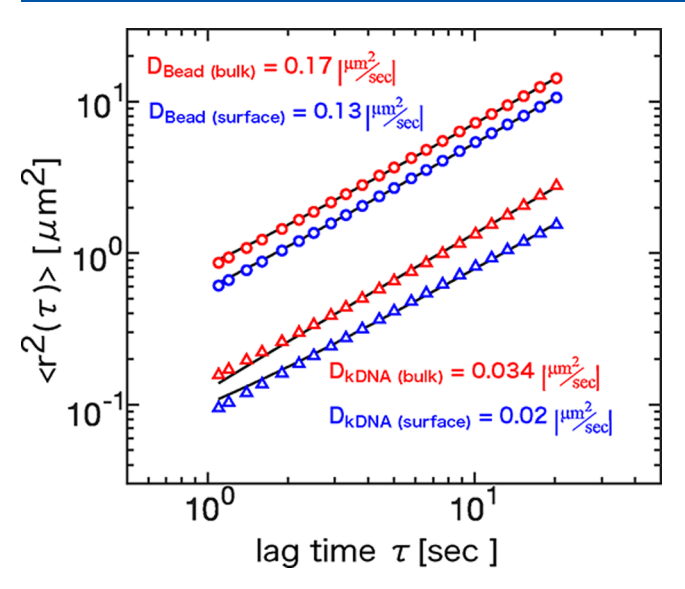


Figure 4. Mean square displacement  $\langle r^2(\tau) \rangle$  versus lag time  $\tau$  for kDNA and polystyrene beads in bulk and on a surface. MSD curves are shown for kDNA (triangles) and 1  $\mu$ m polystyrene beads (circles), with red representing kDNAs (or beads) in bulk and blue representing kDNAs (or beads) on a glass surface. The MSD data is fit to a linear function (solid lines) to extract the diffusion coefficients, as this regime reflects true Brownian diffusion in the relaxed polymeric matrix. The diffusion coefficient in bulk is higher than on the surface, reflecting the reduced mobility of kDNAs near the glass interface due to surface effects. The effective D is derived from the long-time slope.

entities, influenced by depletion interactions with  $\lambda$ -DNA, were pushed toward the surface, where they remained constrained and exhibited two-dimensional surface diffusion with long-lived trajectories. During this motion, some beads transiently stuck to the surface and were categorized as immobile, producing a zero-displacement peak in the van Hove self-correlation function, indicative of particle displacement probabilities (Figure S7, see Supporting Information for details). Focusing on the mobile beads, we observed Gaussian van Hove correlations and Fickian surface diffusion, consistent with Babayekhorasani et al. 52 From their trajectories, we similarly extracted  $\langle r^2( au) \rangle$  and calculated the diffusion coefficient. Notably, the measured diffusion coefficient was significantly reduced compared to bulk values, revealing hindered diffusion near the surface. The ratio  $D_{\text{surface}}$ D<sub>bulk</sub> for spherical beads was 0.75, reflecting this slowdown, which is consistent qualitatively with the hindered diffusion observed by Goldman et al.<sup>53</sup> (see Supporting Information). The quantitative comparison, however, is complicated by the non-Newtonian nature of the medium and the nonuniform surface viscosity resulting from  $\lambda$ - DNA exclusion in the depletion zone. We conducted parallel experiments with kDNA. Like the beads, kDNA was confined to the surface and exhibited hindered, long-lived diffusion. However, the hindrance was even more pronounced ( $D_{\rm surface}/D_{\rm bulk}=0.6$ ), likely due to kDNA's soft and deformable nature, which allows it to adopt a flattened, surface-aligned conformation, thereby enhancing hydrodynamic drag relative to a sphere. Beyond quantifying the slow down of kDNA diffusion on the surface, it is useful to extract a characteristic time scale associated with its dynamics. This time scale corresponds to the time required for a kDNA to diffuse over a distance comparable to its own radius. We find that this takes approximately 96 s, indicating that the key dynamical processes occur on the order of minutes. This time scale, consistent with the data in Figure 3b, provides a natural frame of reference for our experimental observations.

To gain a complete picture of the surface dynamics, we also quantified the in-plane rotational diffusion of individual kDNAs. Figure S8 shows the mean squared angular displacement ( $\langle\Delta\theta^2\rangle$ ) as a function of lag time  $\tau$  for nine individual particles. A linear fit yielded a mean rotational diffusion coefficient of  $D_r=0.0059\pm0.0009~{\rm rad}^2~{\rm s}^{-1}.$  We can compare this rotational time scale to the translational one. The characteristic time for a  $180^\circ$  in-plane reorientation is 840 s. This time scale is significantly longer than the characteristic time for translational diffusion over a particle radius (approximately 96 s). The clear separation between these time scales indicates that translational motion occurs on a faster time scale than full rotational reorientation on the surface.

Pairwise Assembly: Single kDNA to Dimer. *Microscopic Visualization*. Depletion-induced phase separation provides a controlled means to concentrate colloidal dispersions. <sup>54,55</sup> As a fundamental step toward characterizing kDNA–kDNA interactions, we study dimer formation, the simplest yet most informative assembly unit. While the previous section revealed how kDNA-surface depletion induces polar order, we now investigate how depletion forces mediate direct interactions between kDNAs.

kDNAs undergo translational and rotational diffusion on the surface until they come into close proximity. When this happens, their depletion layers overlap, generating the attractive forces described in detail in the Quantitative Analysis section. Once the overlap is sufficiently large such that the depletion interaction exceeds a few  $k_{\rm B}T$  the force becomes strong enough to draw the kDNAs closer.

Super-resolution confocal microscopy snapshots of a kDNA dimer cross-section (Figure 5) reveal phase separation into kDNA-rich and  $\lambda$ -DNA-rich phases driven by depletion interactions induced by the small  $\lambda$ -DNAs ( $R_g=0.7~\mu\mathrm{m}$ ) acting as the depleting agent. Panel (a) shows the kDNA channel (MFP 488 label), panel (b) the  $\lambda$ -DNA channel (Cy5 label), and panel (c) their overlay, highlighting the molecular-level spatial distribution of independently labeled kDNA and  $\lambda$ -DNAs. This dual-labeling technique, which we also apply to larger aggregates (Movie S2), provides direct visualization of the depletion interaction. As shown in Figure 5 and additional experimental figures in the Supporting Information (Figure S9),  $\lambda$ -

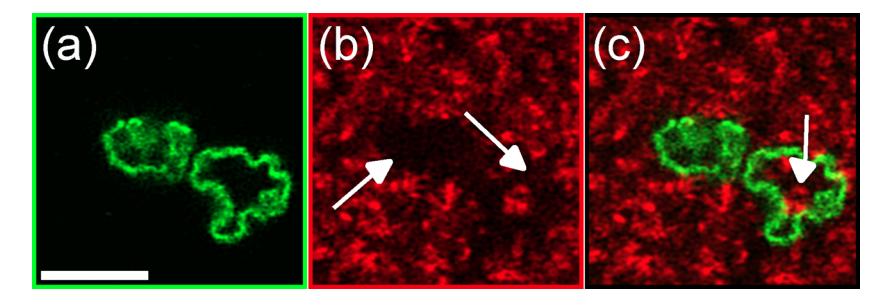
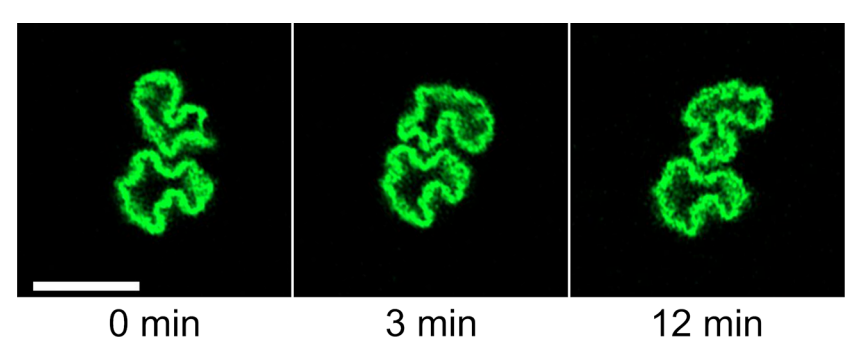


Figure 5. Depletion interaction between kDNA and  $\lambda$ -DNA. We simultaneously imaged fluorescently (a) labeled kDNA (green, MFP488 MIRUS) and (b) fluorescently labeled  $\lambda$ -DNA (red, Cy5). we can see the large dark regions (marked by white arrows) where  $\lambda$ -DNA is depleted. (c) Superposition of images reveals that  $\lambda$ -DNA (white arrow) can reside totally inside the cup-shaped kDNA. However, we have not observed in any of our images  $\lambda$ -DNA threaded through the kDNA surface. The sample consists of 40% stained  $\lambda$ -DNA and 60% unstained  $\lambda$ -DNA. The scalebar is 5 μm.



**Figure 6.** Rotational diffusion and gliding within a kDNA dimer. Time-resolved snapshots of two kDNAs forming a dimer at the surface. The top kDNA undergoes rotational diffusion and glides on the bottom one, progressively optimizing their complementary configuration through depletion interactions. The scalebar is 5  $\mu$ m.

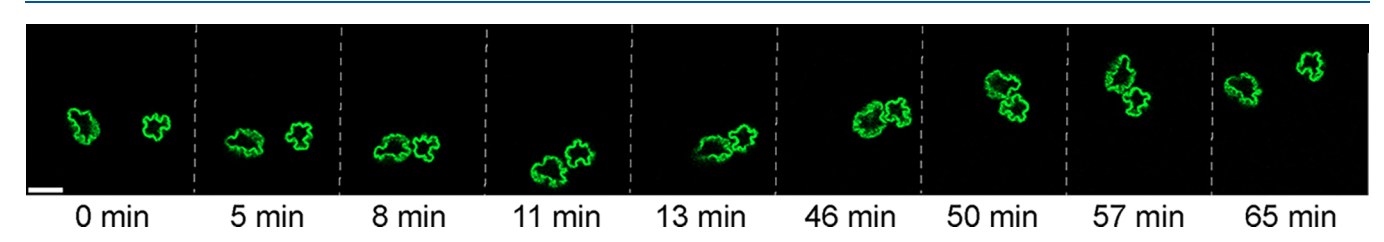
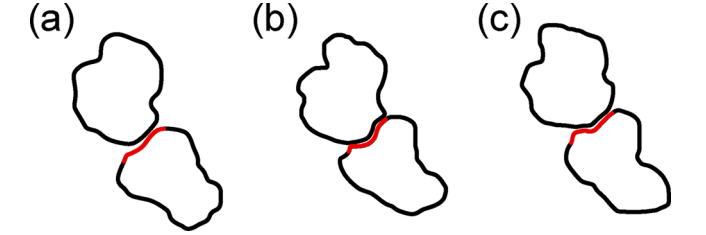


Figure 7. Time-resolved dimerization dynamics mediated by depletion forces. Initially separated (t = 0 min, closest distance 6.5  $\mu$ m), two kDNAs diffuse until their depletion layers, with a thickness of 0.292  $\mu$ m (discussed in detail in the Quantitative Analysis section), overlap at  $t \approx 8$  min, generating an attractive force that increases with excluded volume overlap. Dimerization occurs when the depletion interaction exceeds thermal energy ( $>k_BT$ ). The soft, asymmetric kDNAs then rotate relative to each other for  $\sim$ 50 min, seeking complementary lock-and-key configurations. At  $t \approx 65$  min, rotational misalignment reduces overlap volume, dropping the interaction below  $k_BT$  and causing dissociation. The scale bar is 5  $\mu$ m.

DNAs are largely excluded from kDNA aggregates, promoting kDNA aggregation, though the unique cup-like morphology of kDNA also allows some  $\lambda\text{-DNAs}$  to become trapped within the concave region, a novel observation uniquely enabled by kDNA's morphology. The trapped  $\lambda\text{-DNA}$  is shown by a white arrow in Figure 5c. Notably, we did not observe threading of  $\lambda\text{-DNA}$  through the kDNA network, as  $\lambda\text{-DNA's}$  radius of gyration ( $R_{\rm g}\approx 0.7~\mu\text{m}$ ) is significantly greater than the pristine kDNA network's mesh size ( $\sim\!\!34~\text{nm}$ ),  $^{38,39}$  restricting penetration due to steric constraints, consistent with threading limitations in polymer networks. The lack of threading visualized here through direct dual-labeling microscopy agrees with our indirect assessment from kDNA bulk diffusion analysis, where the measured hydrodynamic radius was consistent with a nonthreading model.

Upon dimerization, kDNAs form a single entity that undergoes coupled rotational and translational diffusion. Initially forming with random alignment, they rearrange dynamically within the dimer: gliding and rotating relative to each other to optimize their contact area into energetically favorable lock-and-key complementary configurations. Figure 6 and Movie S3 shows these dynamics in a kDNA dimer with three snapshots over time. These are cross-sectional images of a dimer on the substrate surface. At t=0, they are bound in a random alignment. The top kDNA turns about 90° clockwise, while the lower one rotates less. By t=12 min, the top kDNA rotates back the other way, counterclockwise, toward its starting alignment. If such rotation reduces the overlap between the two kDNAs, the attraction can weaken below  $\sim k_{\rm B}T$ , causing the dimer to dissociate (Figure 7 and Movie S4); otherwise, it stabilizes and undergoes further rearrangements.

While depletion governs initial assembly, dimer stability is further modulated by the kDNAs' mechanical properties. The kDNAs are intrinsically soft and flexible, with a bending rigidity comparable to vesicle, <sup>56</sup> exhibiting significant thermal fluctuations in their shape. <sup>28,35</sup> During dimerization, this intrinsic softness enables substantial induced bending, each kDNA undergoes cooperative deformation to maximize complementary contact with its partner (Figure 8), consistent with curvature-mediated entropic forces reported by. <sup>27</sup> In their study, hard spheres confined in vesicles were driven toward regions of high membrane curvature due to depletion interactions,



**Figure 8.** Real-time deformation dynamics of flexible kDNAs. Timelapse images (1 s interval) of a dimer showing only the detected kDNA edges, extracted using an edge-detection algorithm. The red region marks the deformed section of the edge. (a) Initial approach phase where kDNAs come within depletion interaction range. (b) Contact-induced bending as the lower kDNA deforms to maximize interfacial complementarity. (C) As the kDNAs separate, the deformed kDNA relaxes back to its original shape, demonstrating the reversibility of depletion-mediated bending and the elasticity of the kDNAs.

analogous to how flexible kDNAs deform to enhance contact area. While individual kDNAs can exhibit undulations, their magnitude is significantly smaller than the large-scale deformations enabled by depletion interactions. To assess the feasibility of this mechanism, we compared the elastic energy penalty for bending with typical depletion gains. We considered two different estimates for the bending rigidity  $\kappa$ of kDNA networks reported in the literature, both inferred indirectly from experiments rather than directly measured. A scaling analysis using the Helfrich free energy model calculated bending penalties of ~0.04–0.6  $k_{\rm B}T$  for the lower estimate  $(\kappa = 3 \times 10^{-21} \, \rm J)^{38}$  and ~3–32  $k_{\rm B}T$  for the higher estimate  $(\kappa = 1.8 \times 10^{-19} \, \rm J)^{.28}$  These bounds provide a plausible range for the bending energy penalty. As quantified in Quantitative Analysis section, the measured depletion interactions in our system for different dimers can overcome these bending costs. This confirms that depletion attraction is sufficient to drive the observed deformations, as directly visualized by the characteristic bending of kDNA edges in our experimental images

(Figure S10). Such adaptive reshaping increases effective binding stiffness, stabilizing lock-and-key binding compared to rigid systems. However, despite this enhanced stability, the interactions remain relatively weak and sensitive to thermal perturbations, leading to dynamic rearrangements over time.

Figure 9 directly captures the interplay between depletion strength and thermal fluctuations: dimers dissociate when their interaction

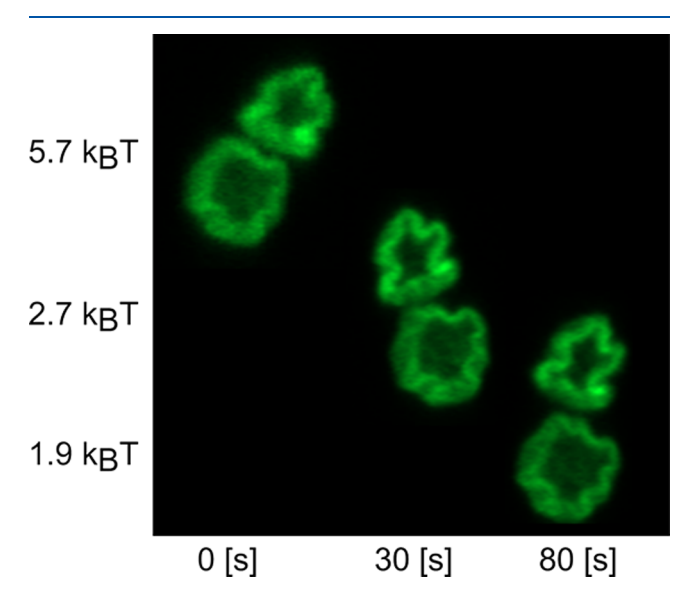


**Figure 9.** Evolution of depletion interaction energy in a dissociating dimer. The vertical axis shows the interaction strength at each time point. Depletion interaction energy  $(k_{\rm B}T)$  decreases as the dimer dissociates over time (0, 30, and 80 s). Z-stacks were processed using Fiji's Z-project function to generate top-view dimer images. The increasing separation reduces excluded volume overlap, weakening the depletion attraction. In the following section, we discuss in detail how these interaction strengths were quantitatively estimated.

energy nears  $\sim k_{\rm B}T$ . This occurs when rotational misalignment or separation reduces depletion-layer overlap, weakening attraction until thermal effects dominate. The process is reversible, dissociated kDNAs may rebind if diffusion brings them into proximity under favorable depletion conditions.

Quantitative Analysis. When kDNAs are dispersed in a solution containing nonadsorbing polymers, the configurational entropy of the polymer chains is reduced near the kDNA surfaces, leading to negative adsorption. As a result, depletion layers form around the kDNAs, characterized by a lower polymer concentration compared to the bulk solution. The presence of these depletion layers gives rise to an effective attractive depletion force between the kDNAs. When the depletion layers of two kDNAs overlap, the excluded volume accessible to the polymer chains increases. As a result, the system minimizes its free energy by favoring configurations in which the kDNAs are in close proximity. This phenomenon effectively induces an attraction between the kDNAs, even though the direct kDNAkDNA interaction is purely repulsive as kDNA is negatively charged with a measured zeta potential of  $-70 \pm 4$  mV.<sup>40</sup> To quantify this interaction, we consider the osmotic pressure of polymers as depleting agent following the classic work of Asakura and Oosawa<sup>1</sup>:

$$W_{\text{dep}}(h) = \begin{cases} \infty & h < 0 \\ -\Pi_{\text{p}}V_{\text{ov}}(h) & 0 \le h \le 2R_{\text{p}} \\ 0 & h > 2R_{\text{p}} \end{cases}$$
(1)

where h represents the separation distance between two kDNAs,  $W_{\rm dep}(h)$  is depletion interaction potential at distance h,  $V_{\rm ov}$  is the overlap excluded volume,  $R_{\rm p}$  is the effective hard-sphere radius that describes the polymer and  $\Pi_{\rm p}$  is the  $\lambda$ -DNA osmotic pressure. In

general, the overlap volume  $V_{\rm ov}(h)$  depends on particle geometry. However, since the kDNA's geometry is irregular and poorly defined, we cannot derive an explicit expression for  $V_{\rm ov}(h)$  in this case. Therefore, we find the overlap using the experimental images and then multiply by the osmotic pressure to estimate the associated depletion energy.

When the polymer concentration in the solution exceeds the overlap concentration,  $c^*$ , the solution enters the semidilute regime where the polymer's behavior is characterized by a correlation length  $\xi$ , replacing the radius of gyration as the relevant length scale. Here,  $\xi$  represents the average spacing between entanglement points or, equivalently, the size of a blob within which a section of the polymer chain still behaves as an independent coil. Consequently, the depletion mechanism known from hard-sphere and dilute polymer systems remains applicable in semidilute solutions if the background fluid is modeled as an ideal gas of spherical blobs. In our experiments, the  $\lambda$ -DNA concentration is 100  $\mu$ g mL<sup>-1</sup>, which corresponds to 2.4  $c^*$ . The osmotic pressure of  $\lambda$ -DNA solutions has been measured for different  $\lambda$ -DNA concentrations by Verma et al. Based on their study, our concentration of  $\lambda$ -DNA falls within the semidilute regime (the crossover concentration is expected to be 30–50  $\mu$ g mL<sup>-158</sup>), where we define  $R_p$  as

$$R_p = (\pi/2)\xi \tag{2}$$

For the  $\lambda$ -DNA concentration used in our experiment,  $R_{\rm p}=0.29~\mu{\rm m}^{57}$  and  $\xi=0.18~\mu{\rm m}$ . The osmotic pressure for this system was experimentally determined as  $\Pi_{\rm p}/k_{\rm B}T=3~\mu{\rm m}^{-3},^{57}$  combining this result with eq 1 gives

$$W_{\text{dep}}(h) = -3k_{\text{B}}T \times V_{\text{ov}}(h) \quad 0 \le h \le \pi \xi \tag{3}$$

where  $V_{\rm ov}$  has units of  $\mu{\rm m}^3$ . To quantify depletion forces between dimerized kDNA, we performed 3D confocal imaging and analyzed the excluded volume overlap (Figure 10). First, we binarized each z-

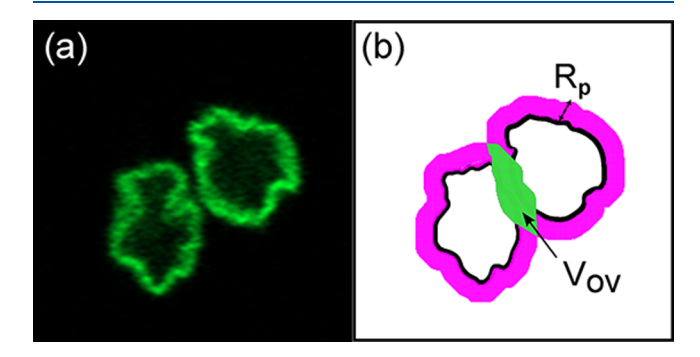


Figure 10. Cross-sectional analysis of dimer configurations and depletion interactions. (a) Confocal microscopy image of a single cross section (z-position) of a dimer with both kDNAs in a base down orientation. (b) Binarized representation of the cross section, highlighting the depletion layer (magenta) induced by  $\lambda$ -DNA in the surrounding fluid. The green region denotes the overlap-excluded area, where the depletion layers of the two kDNAs intersect, illustrating the effective interaction potential arising from depletion forces. The depletion layer arises due to the exclusion of  $\lambda$ -DNA from the narrow gap between the kDNAs, leading to an attractive force between them.

slice of the confocal stack to identify kDNA edges using MATLAB. We then defined the depletion layer (magenta shading in Figure 10b) as the region within one  $R_{\rm p}$  of each kDNA surface. The overlapping excluded volumes (green areas in Figure 10b) were calculated slice-by-slice and summed across all z-positions to determine the total overlap excluded volume. This approach is analogous to the Derjaguin approximation, which integrates local interactions between curved surfaces by decomposing them into infinitesimal parallel slices. S9 Here, we apply a similar principle by summing the depletion overlap

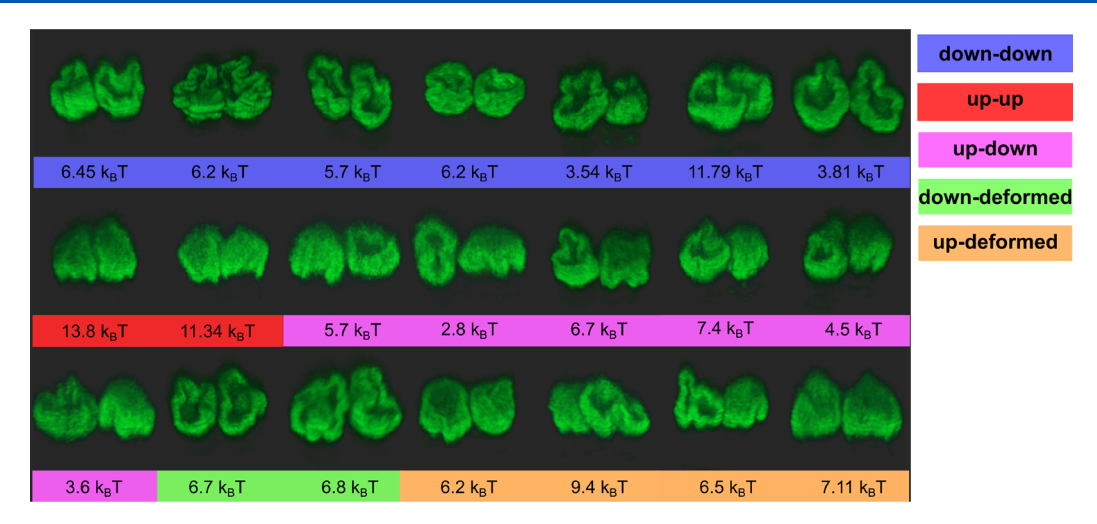


Figure 11. Configurations and depletion strengths of dimers formed via depletion interactions in the presence of  $\lambda$ -DNA. The dimers exhibit various orientations, including base down—base down (down—down), base up—base up (up—up), base up—base down (up—down), base down—deformed (down-deformed) and base up-deformed (up-deformed) as visualized through 3D confocal microscopy images. 3D images were reconstructed using Imaris and tilted slightly for perspective. The depletion interaction strength for each configuration, which is proportional to the excluded volume overlap (calculated under the assumption of a semidilute polymer regime with a depletion layer thickness of  $R_{\rm p}$ ), is indicated below each dimer.

contributions from each 2D cross-section to reconstruct the 3D interaction volume.

Figure 11 presents a representative set of 21 dimers and their corresponding calculated interaction energies. Based on their orientations and structural features, we have categorized dimers into five different categories: down–down, up–up, up–down, down-deformed, and up-deformed. As mentioned earlier, some kDNAs do not adopt a clear base-up or base-down shape when isolated. Instead, they undergo structural perturbations when they are in bulk that lead to deformed or buckled conformations. we call them deformed kDNA. These deformed kDNAs contribute to the diversity observed in dimer structures. Examples of such buckled conformations are provided in Figure S11. These structural variations result in a range of interaction strengths, with measured depletion energies spanning from 2.8 to 13.8  $k_{\rm B}T$ , consistent with prior experimental studies of spherical particles in similar  $\lambda$ -DNA systems.  $^{60}$ 

While these classifications highlight clear structural differences between dimers, statistically we cannot draw strong conclusions about differences in interaction energy based solely on configuration. No clear trend in depletion strength emerged based solely on kDNA orientations within dimers, for example, up—up pairs (13.8–11.34  $k_{\rm B}T$ ) showed roughly similar depletion strength to some down—down pairs (e.g., 11.79  $k_{\rm B}T$ ). This indicates that the interaction is largely independent of individual kDNA orientation and instead arises from geometrical features: as long as the pairing maximizes excluded volume overlap, the specific way two kDNAs orient with respect to the surface does not greatly matter. Figure 12 summarizes the distribution of interaction energies via a histogram with an overlaid rug plot. The broad, continuous spread of energies highlights the absence of discrete energy levels correlating with the kDNA orientation within dimers.

Generally, dimer depletion interactions are weak, typically on the order of a few  $k_{\rm B}T$ , confirming that dimers are metastable and dynamic. During experiments, we observe frequent formation and dissociation of dimers, consistent with the relatively low binding energies that allow for reversible assembly. Stronger bonds form when two kDNA with curved surfaces with opposite curvatures (positivenegative) interlock, akin to a lock-and-key mechanism, which boosts overlap in the xy-plane and enhances depletion (Figure 13, strong interaction panel). In contrast, pairings with matching curvatures (both positive or both negative) yield the weakest interactions (Figure 13, weak interaction panel). Overall, the total depletion strength scales with both the per-plane overlap (how well surfaces fit in each cross-section) and the number of contributing z-planes (dimer height

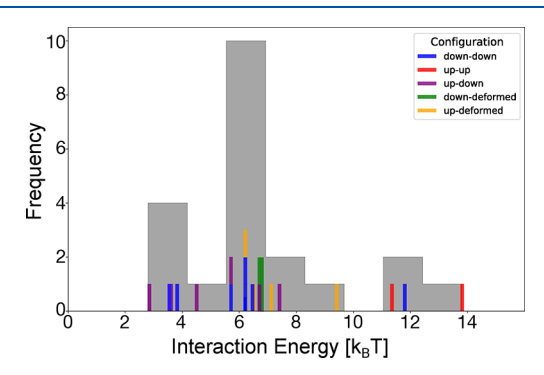


Figure 12. Distribution of depletion interaction energies across 21 kDNA dimers. The histogram shows the overall frequency of measured energies (in  $k_{\rm B}T$ ). An overlaid rug plot (vertical ticks) marks individual data points, revealing a spread from 2.8 to 13.8  $k_{\rm B}T$ . Since some dimers have exactly the same interaction energy, their rug plot marks overlap. To make this clear, the associated tick on the rug plot is represented with multiple colors, where the relative length of each color segment corresponds to the number of dimers with that energy. For instance, three dimers have an energy of  $6.2~k_{\rm B}T$  with two of them are in a down—down configuration, resulting in 2/3 of the tick being blue and one is in a up-deformed configuration, shown in yellow on the rug plot.

along the z-axis) (Figure 13). Flattened dimers, even with good fits in some planes, weaken due to fewer overlapping z-planes, while taller, well-matched dimers achieve maximum strength by pairing optimal xy fits with extended z-overlap. We benchmark the depletion strength against the Asakura-Oosawa model for hard spheres of comparable size in a semidilute nonadsorbing polymer solution. For two hard spheres of radius  $R = 2.5 \mu m$  under our experimental  $\lambda$ -DNA depletant conditions (polymer's effective hard-sphere radius  $R_p = 0.29$  $\mu$ m, correlation length  $\xi = 0.186 \ \mu$ m, osmotic pressure  $\Pi = 3 \ k_B T$  $\mu$ m<sup>-3</sup>), the depletion potential yields a well depth of  $\approx 4 k_B T$ , placing our system in the weak, dimer-forming regime ( $\sim$ 2.8–13.8  $k_BT$ ) typical of reversible attractions in hard-sphere/polymer mixtures. However, the complex shapes of kDNAs make analytical predictions challenging; we therefore compare our results to simplified geometries (spheres, disks, rectangles) in the Supporting Information (Figure S12). Following the estimation of kDNA-kDNA interactions, we estimated the depletion energy binding a kDNA to the surface. As

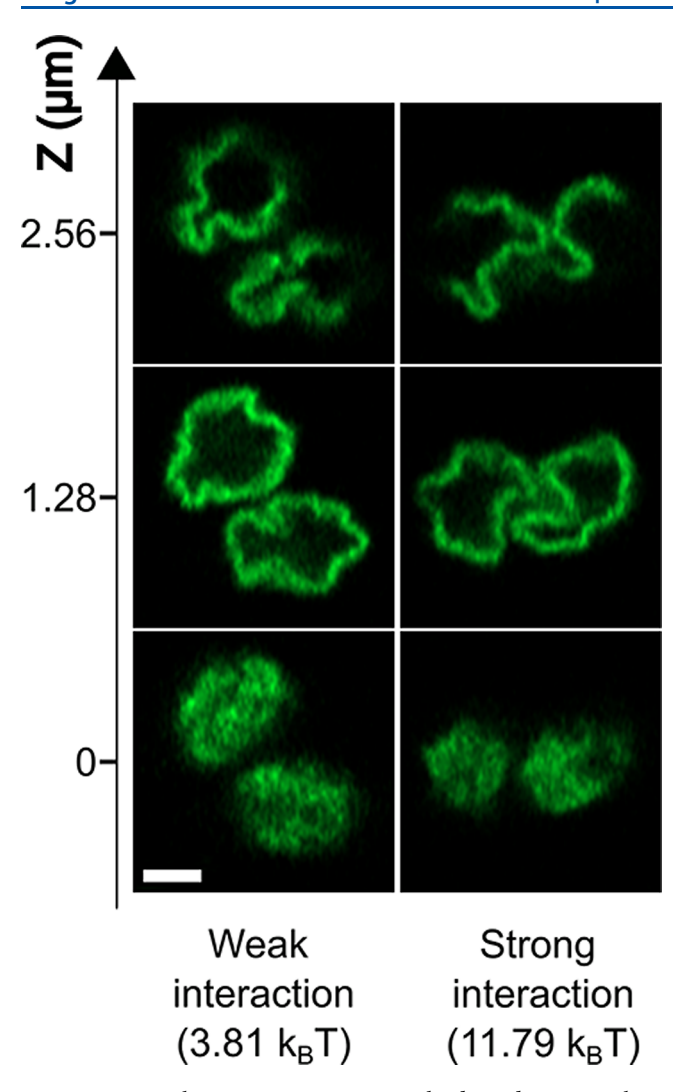


Figure 13. Depletion interaction strength depends on xy-plane overlap and z-plane continuity. Left column: Dimer with weak depletion interaction show poor xy-plane fitting and reduced excluded-volume overlap across z-sections. Right column: Dimer with strong interaction exhibit close curvature matching in the xy-plane and higher overlap, maintained over multiple z-sections (spaced at 1.28  $\mu$ m). Scale bar: 2  $\mu$ m.

detailed in the Supporting Information, this kDNA-surface interaction has a strength of approximately  $\sim\!42~k_{\rm B}T$  for a kDNA modeled as a disk at an average distance from the glass slide of 13.6 nm, significantly stronger than the inter-kDNA attractions and confirming why kDNAs bind irreversibly to the surface.

## CONCLUSIONS

This study provides a quantitative analysis of depletion interactions between soft, asymmetric kDNAs in the presence of linear  $\lambda$ -DNA, utilizing a combined approach of confocal microscopy and the Asakura–Oosawa (AO) model. Studying kDNA dimers adsorbed on a flat surface provides a platform where we can clearly observe the conformations of the colloidal entities and perform quantitative long-term microscopy to track their conformation and dynamics. We have systematically characterized the strength of depletion interactions between kDNA pairs across a variety of relative orientations, marking an advancement in understanding entropic forces between anisotropic soft colloidal entities.

Our findings reveal that depletion forces significantly affect kDNA's organization, orientation, and dynamics at interfaces. Specifically, λ-DNA induces kDNA adsorption to surfaces through depletion interactions, resulting in a persistent basedown polar alignment. The surface-confined kDNA molecules retain high mobility, undergoing sustained two-dimensional (2D) diffusion and facilitating dynamic interactions. This quasi-2D confinement reduces the diffusion coefficient by 1.6× compared to bulk solution, and facilitates high-precision tracking of the dimerization processes that would otherwise be challenging to resolve in three dimensions.

The surface-mediated assembly of kDNA highlights distinctive interfacial dynamics. Individual kDNA molecules diffuse freely until entering mutual interaction ranges, wherein depletion forces drive spontaneous dimer formation. The anisotropic shape of kDNA, coupled with 2D diffusion, results in highly dynamic dimers that glide, rotate, and reconfigure to optimize conformal contact. This behavior reflects an energy landscape shaped by depletion forces and interfacial constraints, where persistent diffusion and depletion attraction establish dynamic equilibria. Dimers maintain aligned configurations while exhibiting translational and rotational motion, underscoring the unique interplay of mobility and attraction in this system.

In the  $\lambda$ -DNA solutions, arising depletion forces are the key mechanism controlling kDNA's behavior at interfaces, mediating adsorption, orientation, and dimer formation kinetics. In contrast, our prior work (Yadav et al.<sup>37</sup>) found that 10 kDa PEG, with a 2 nm radius of gyration much smaller than kDNA's 34 nm mesh size, penetrates the kDNA network, inducing intramolecular aggregation, leading to a flat-toglobule phase transition driven by configurational entropy. These contrasting results highlight the relative depletant size in comparison with the kDNA pore size as critical for entropic interactions. This insight can inform soft-matter systems, enabling design of reconfigurable materials. Future research should be done to systematically change the molecular weight of the linear DNA depletant to more firmly establish the ratio of depletant size to kDNA mesh size as a key dimensionless group. Other polymeric depletants, such as dextran, could also prove useful.

Our studies showed that the flexibility of the kDNA was an important attribute allowing it to adapt to its environment. Future research could explore the modulation of kDNA softness by enzymatic digestion to systematically alter mechanical properties. Such studies could bridge biological and engineered colloidal systems, enhancing our ability to design adaptive materials. By elucidating the interplay between softness, curvature, and depletion forces, this work lays a foundation for the advancement of programmable self-assembly in soft matter.

# ASSOCIATED CONTENT

# Supporting Information

ı

The Supporting Information is available free of charge at https://pubs.acs.org/doi/10.1021/acs.langmuir.5c04422.

Investigation of gravity effect on kDNA sedimentation; tracking kDNA's orientation over time to verify they maintain their orientation; 3D reconstructed images of kDNA in both base up and base down orientation and their cross section on the surface; additional example of kDNA trajectory on the surface; calculation of von Hove

correlation for both kDNA and bead on the surface and in bulk; calculation of solution viscosity in the presence of  $\lambda$ -DNA; schematic illustrating kDNA with and without penetration of lambda DNA into kDNA; hindered diffusion of kDNA; rotational diffusion of kDNA; dual visualization of kDNA and  $\lambda$ -DNA; bending energy penalty; 3D reconstructed images of kDNA in a buckled configuration; and theoretical estimation of depletion forces using spheres/disks/rectangular approximations (PDF)

Comparative dynamics of kDNA in bulk solution and on a surface in the presence of  $\lambda$ -DNA (AVI)

Dual visualization of kDNA and  $\lambda$ -DNA in high concentration of kDNA (MP4)

Rotational diffusion and gliding of a kDNA dimer (AVI) kDNA dimerization dynamics (AVI)

#### AUTHOR INFORMATION

# **Corresponding Author**

Patrick S. Doyle — Department of Chemical Engineering, Massachusetts Institute of Technology, Cambridge, Massachusetts 02139, United States; oocid.org/0000-0003-2147-9172; Email: pdoyle@mit.edu

#### Authors

Zahra Zarei — Department of Chemical Engineering, Massachusetts Institute of Technology, Cambridge, Massachusetts 02139, United States

Indresh Yadav – Department of Physics, Indian Institute of Technology Bhubaneswar, Bhubaneswar, Odisha 752050, India

Complete contact information is available at: https://pubs.acs.org/10.1021/acs.langmuir.5c04422

# Notes

The authors declare no competing financial interest.

#### ACKNOWLEDGMENTS

We acknowledge partial support from the National Science Foundation grant CBET-2510937 to PSD. We thank the Whitehead Institute Microscopy Facility for technical assistance with confocal microscopy and gratefully acknowledge Asier Marcos Vidal for their expert guidance.

# REFERENCES

- (1) Asakura, S.; Oosawa, F. On interaction between two bodies immersed in a solution of macromolecules. *J. Chem. Phys.* **1954**, 22, 1255–1256.
- (2) Fåhraeus, R. The suspension stability of the blood. *Physiol. Rev.* **1929**, *9*, 241–274.
- (3) Gonzalez La Corte, S.; Stevens, C. A.; Cárcamo-Oyarce, G.; Ribbeck, K.; Wingreen, N. S.; Datta, S. S. Morphogenesis of bacterial cables in polymeric environments. *Sci. Adv.* **2025**, *11*, No. eadq7797.
- (4) Sept, D.; McCammon, J. A. Thermodynamics and kinetics of actin filament nucleation. *Biophys. J.* **2001**, *81*, *667–674*.
- (5) Dickinson, R. B.; Caro, L.; Purich, D. L. Force generation by cytoskeletal filament end-tracking proteins. *Biophys. J.* **2004**, *87*, 2838–2854.
- (6) Hosek, M.; Tang, J. X. Polymer-induced bundling of F actin and the depletion force. *Phys. Rev. E:Stat., Nonlinear, Soft Matter Phys.* **2004**, *69*, No. 051907.
- (7) Marenduzzo, D.; Micheletti, C.; Cook, P. R. Entropy-driven genome organization. *Biophys. J.* **2006**, *90*, 3712–3721.

- (8) Michaels, T. C.; Qian, D.; Šarić, A.; Vendruscolo, M.; Linse, S.; Knowles, T. P. Amyloid formation as a protein phase transition. *Nat. Rev. Phys.* **2023**, *5*, 379–397.
- (9) Royall, C. P.; Faers, M. A.; Fussell, S. L.; Hallett, J. E. Real space analysis of colloidal gels: Triumphs, challenges and future directions. *J. Phys.:Condens. Matter* **2021**, *33*, No. 453002.
- (10) Biancaniello, P. L.; Kim, A. J.; Crocker, J. C. Colloidal interactions and self-assembly using DNA hybridization. *Phys. Rev. Lett.* **2005**, 94, No. 058302.
- (11) Kim, A. J.; Biancaniello, P. L.; Crocker, J. C. Engineering DNA-mediated colloidal crystallization. *Langmuir* **2006**, 22, 1991–2001.
- (12) Aldaye, F. A.; Sleiman, H. F. Dynamic DNA templates for discrete gold nanoparticle assemblies: control of geometry, modularity, write/erase and structural switching. *J. Am. Chem. Soc.* **2007**, 129, 4130–4131.
- (13) Park, S. Y.; Lytton-Jean, A. K.; Lee, B.; Weigand, S.; Schatz, G. C.; Mirkin, C. A. *Spherical Nucleic Acids*; Jenny Stanford Publishing, 2020; pp 515–525.
- (14) Leunissen, M. E.; Dreyfus, R.; Sha, R.; Wang, T.; Seeman, N. C.; Pine, D. J.; Chaikin, P. M. Towards self-replicating materials of DNA-functionalized colloids. *Soft Matter* **2009**, *5*, 2422–2430.
- (15) Novak, J. P.; Feldheim, D. L. Assembly of phenylacetylene-bridged silver and gold nanoparticle arrays. *J. Am. Chem. Soc.* **2000**, 122, 3979–3980.
- (16) Breed, D. R.; Thibault, R.; Xie, F.; Wang, Q.; Hawker, C. J.; Pine, D. J. Functionalization of polymer microspheres using click chemistry. *Langmuir* **2009**, *25*, 4370–4376.
- (17) Leunissen, M. E.; Dreyfus, R.; Cheong, F. C.; Grier, D. G.; Sha, R.; Seeman, N. C.; Chaikin, P. M. Switchable self-protected attractions in DNA-functionalized colloids. *Nat. Mater.* **2009**, *8*, 590–595.
- (18) Rossi, L.; Sacanna, S.; Irvine, W. T.; Chaikin, P. M.; Pine, D. J.; Philipse, A. P. Cubic crystals from cubic colloids. *Soft Matter* **2011**, *7*, 4139–4142.
- (19) Lee, S. H.; Gerbode, S. J.; John, B. S.; Wolfgang, A. K.; Escobedo, F. A.; Cohen, I.; Liddell, C. M. Synthesis and assembly of nonspherical hollow silica colloids under confinement. *J. Mater. Chem.* **2008**, *18*, 4912–4916.
- (20) Sacanna, S.; Rossi, L.; Wouterse, A.; Philipse, A. P. Observation of a shape-dependent density maximum in random packings and glasses of colloidal silica ellipsoids. *J. Phys.:Condens. Matter* **2007**, *19*, No. 376108
- (21) Sacanna, S.; Rossi, L.; Kuipers, B.; Philipse, A. Fluorescent monodisperse silica ellipsoids for optical rotational diffusion studies. *Langmuir* **2006**, 22, 1822–1827.
- (22) Avendaño, C.; Escobedo, F. A. Packing, entropic patchiness, and self-assembly of non-convex colloidal particles: A simulation perspective. *Curr. Opin. Colloid Interface Sci.* **2017**, *30*, 62–69.
- (23) Zhao, K.; Mason, T. G. Directing colloidal self-assembly through roughness-controlled depletion attractions. *Phys. Rev. Lett.* **2007**, 99, No. 268301.
- (24) Sacanna, S.; Irvine, W. T.; Chaikin, P. M.; Pine, D. J. Lock and key colloids. *Nat.* **2010**, *464*, 575–578.
- (25) Marechal, M.; Kortschot, R. J.; Demirörs, A. F.; Imhof, A.; Dijkstra, M. Phase behavior and structure of a new colloidal model system of bowl-shaped particles. *Nano Lett.* **2010**, *10*, 1907–1911.
- (26) Ashton, D. J.; Jack, R. L.; Wilding, N. B. Self-assembly of colloidal polymers via depletion-mediated lock and key binding. *Soft Matter* **2013**, *9*, 9661–9666.
- (27) Dinsmore, A.; Wong, D.; Nelson, P.; Yodh, A. Hard spheres in vesicles: curvature-induced forces and particle-induced curvature. *Phys. Rev. Lett.* **1998**, *80*, 409.
- (28) Klotz, A. R.; Soh, B. W.; Doyle, P. S. Equilibrium structure and deformation response of 2D kinetoplast sheets. *Proc. Natl. Acad. Sci. U.S.A.* **2020**, *117*, 121–127.
- (29) Soh, B. W.; Doyle, P. S. Equilibrium conformation of catenated DNA networks in slitlike confinement. *ACS Macro Lett.* **2021**, *10*, 880–885.

- (30) Polson, J. M.; Garcia, E. J.; Klotz, A. R. Flatness and intrinsic curvature of linked-ring membranes. *Soft Matter* **2021**, *17*, 10505–10515
- (31) Chen, J.; Rauch, C. A.; White, J. H.; Englund, P. T.; Cozzarelli, N. R. The topology of the kinetoplast DNA network. *Cell* **1995**, *80*, 61–69.
- (32) Chen, J.; Englund, P. T.; Cozzarelli, N. R. Changes in network topology during the replication of kinetoplast DNA. *EMBO Journal* **1995**, *14*, 6339–6347.
- (33) Michieletto, D.; Marenduzzo, D.; Orlandini, E. Is the kinetoplast DNA a percolating network of linked rings at its critical point? *Phys. Biol.* **2015**, *12*, No. 036001.
- (34) Ibrahim, L.; Liu, P.; Klingbeil, M.; Diao, Y.; Arsuaga, J. Estimating properties of kinetoplast DNA by fragmentation reactions. *J. Phys. A:Math. Theor.* **2019**, *52*, No. 034001.
- (35) Yadav, I.; Al Sulaiman, D.; Doyle, P. S. Tuning the topology of a two-dimensional catenated DNA network. *Phys. Rev. Res.* **2023**, *S*, No. 013141.
- (36) Soh, B. W.; Khorshid, A.; Al Sulaiman, D.; Doyle, P. S. Ionic effects on the equilibrium conformation of catenated DNA networks. *Macromolecules* **2020**, *53*, 8502–8508.
- (37) Yadav, I.; Al Sulaiman, D.; Soh, B. W.; Doyle, P. S. Phase transition of catenated DNA networks in poly (ethylene glycol) solutions. ACS Macro Lett. 2021, 10, 1429–1435.
- (38) He, P.; Katan, A. J.; Tubiana, L.; Dekker, C.; Michieletto, D. Single-molecule structure and topology of kinetoplast DNA networks. *Phys. Rev. X* **2023**, *13*, No. 021010.
- (39) Diggines, B.; Whittle, S.; Yadav, I.; Holmes, E. P.; Rollins, D. E.; Catley, T. E.; Doyle, P. S.; Pyne, A. L. Multiscale topological analysis of kinetoplast DNA via high-resolution AFM. *Phys. Chem. Chem. Phys.* **2024**, *26*, 25798–25807.
- (40) Yadav, I.; Doyle, P. S. Phase behavior of catenated-linear DNA mixtures. *Soft Matter* **2025**, *21*, 6919–6929.
- (41) Khanal, P.; Peddireddy, K. R.; Marfai, J.; McGorty, R.; Robertson-Anderson, R. M. DNA topology dictates emergent bulk elasticity and hindered macromolecular diffusion in DNA-dextran composites. *J. Rheol.* **2022**, *66*, 699–715.
- (42) Dietrich, C.; Angelova, M.; Pouligny, B. Adhesion of latex spheres to giant phospholipid vesicles: statics and dynamics. *J. Phys. II* **1997**, *7* (11), 1651–1682.
- (43) Deserno, M.; Gelbart, W. M. Adhesion and wrapping in colloid-vesicle complexes. *J. Phys. Chem. B* **2002**, *106*, 5543–5552.
- (44) Noguchi, H.; Takasu, M. Adhesion of nanoparticles to vesicles: a Brownian dynamics simulation. *Biophys. J.* **2002**, *83*, 299–308.
- (45) Boulbitch, A. Enforced unbinding of a bead adhering to a biomembrane by generic forces. *Europhys. Lett.* **2002**, *59*, 910.
- (46) Onuh, G.; Harries, D.; Manor, O. Depletion-Induced Self-Assembly of Colloidal Particles on a Solid Substrate. *Langmuir* **2024**, 40, 8554–8561.
- (47) Karas, A. S.; Glaser, J.; Glotzer, S. C. Using depletion to control colloidal crystal assemblies of hard cuboctahedra. *Soft Matter* **2016**, 12, 5199–5204.
- (48) Sabapathy, M.; Kalapurakal, R. A. M.; Mani, E. Self-assembly of inverse patchy colloids with tunable patch coverage. *Phys. Chem. Chem. Phys.* **2017**, *19*, 13122–13132.
- (49) Kim, D.; Bae, W. K.; Kim, S.-H.; Lee, D. C. Depletion-mediated interfacial assembly of semiconductor nanorods. *Nano Lett.* **2019**, *19*, 963–970.
- (50) Dogic, Z.; Fraden, S. Ordered phases of filamentous viruses. Curr. Opin. Colloid Interface Sci. 2006, 11, 47–55.
- (51) Zhu, X.; Kundukad, B.; van der Maarel, J. R. Viscoelasticity of entangled λ-phage DNA solutions. *J. Chem. Phys.* **2008**, *129*, 185103.
- (52) Babayekhorasani, F.; Dunstan, D. E.; Krishnamoorti, R.; Conrad, J. C. Nanoparticle diffusion in crowded and confined media. *Soft Matter* **2016**. *12*. 8407–8416.
- (53) Goldman, A. J.; Cox, R. G.; Brenner, H. Slow viscous motion of a sphere parallel to a plane wall—I Motion through a quiescent fluid. *Chem. Eng. Sci.* **1967**, *22*, 637–651.

- (54) Yadav, I.; Aswal, V. K.; Kohlbrecher, J. Size-dependent interaction of silica nanoparticles with lysozyme and bovine serum albumin proteins. *Phys. Rev. E* **2016**, *93*, No. 052601.
- (55) Yadav, I.; Kumar, S.; Aswal, V. K.; Kohlbrecher, J. Structure and interaction in the pH-dependent phase behavior of nanoparticle—protein systems. *Langmuir* **2017**, *33*, 1227–1238.
- (56) Rossier, O.; Cuvelier, D.; Borghi, N.; Puech, P.; Derényi, I.; Buguin, A.; Nassoy, P.; Brochard-Wyart, F. Giant vesicles under flows: Extrusion and retraction of tubes. *Langmuir* **2003**, *19*, 575–584.
- (57) Verma, R.; Crocker, J. C.; Lubensky, T. C.; Yodh, A. G. Entropic colloidal interactions in concentrated DNA solutions. *Phys. Rev. Lett.* **1998**, *81*, 4004.
- (58) Pernodet, N.; Tinland, B. Influence of  $\lambda$ -DNA concentration on mobilities and dispersion coefficients during agarose gel electrophoresis. *Biopolymers: Original Research on Biomolecules* **1997**, 42, 471–478
- (59) Derjaguin, B. Untersuchungen ueber die reibung und adhaesion, IV: Theorie des anhaftens kleiner teilchen. *Kolloid-Z.* **1934**, *69*, 155–164.
- (60) Verma, R.; Crocker, J. C.; Lubensky, T. C.; Yodh, A. Attractions between hard colloidal spheres in semiflexible polymer solutions. *Macromolecules* **2000**, *33*, 177–186.
- (61) Nabizadeh, M.; Nasirian, F.; Li, X.; Saraswat, Y.; Waheibi, R.; Hsiao, L. C.; Bi, D.; Ravandi, B.; Jamali, S. Network physics of attractive colloidal gels: Resilience, rigidity, and phase diagram. *Proc. Natl. Acad. Sci. U. S. A.* **2024**, *121*, No. e2316394121.
- (62) Dibble, C. J.; Kogan, M.; Solomon, M. J. Structure and dynamics of colloidal depletion gels: Coincidence of transitions and heterogeneity. *Phys. Rev. E:Stat., Nonlinear, Soft Matter Phys.* **2006**, 74, No. 041403.

